Characterization of Energy Deposition and Outgoing Particles for W, Hg and UCx targets[1]

A. Plukis[a,b] and D. Ridikas[a]

[a]CEA Saclay, F-91911 Gif-sur-Yvette, France
[b]IPN Orsay, F-91406 Orsay Cedex, France
E-mail : ridikas@cea.fr; fax: +33 1 69087584

In the frame of the EURISOL project [1] we present calculations of 1 GeV proton beam interacting with different targets. Natural tungsten, mercury and UC_x are considered as target materials. Total energy deposition including its spatial distributions all over the target are given. In addition, outgoing particle (p, n, ?) energy spectra and angular distributions are provided.

Introduction

It seems that an increase of primary beam intensity does not necessarily increase the intensity of the secondary RNBs as was discussed in [2]. The authors argue that the maximum RNBs will be obtained actually for a limited incident beam power. This is an important warning that there might be quite severe limitations with respect to the admissible power on the target. For the RNB facilities based on the charged particle induced reactions, this limitation is of the order of ~20-30kW in the RNB production target. An alternative way of producing the RNBs in the mass region of 75<A<160 can be achieved utilizing a target-converter (neutron source). The emitted neutrons then interact with a fissionable target. Contrary to the charged particles, the neutrons will heat the target indirectly and mainly by the "useful" fission reactions.

In this work we calculate the energy deposited by 1GeV protons (at 1MW incident beam power) and also by all secondary particles both in the RNB production targets (UC_x) as well as in potential targets-converters (^{nat}W and ^{nat}Hg) for neutron production in the case of different geometry considerations. Both longitudinal and radial energy deposit distributions are given including outgoing particle (p, n, ?) energy and angular dependence. The results are supposed to serve for the target heat calculations, a geometry optimization for the RNB production and/or a neutron production targets as well as for radioprotection purposes.

Description of simulations

All calculations are done with the MCNPX multi-particle transport code [3]. As a rule, the LANL T-2 neutron libraries up to 150 MeV have been used, while for higher energies theoretical models within MCNPX have been employed. These include the ISABEL intra-nuclear cascade model and the ORNL evaporation-fission model [3]. As no high energy data library exists for uranium , the ENDF-VI data files up to 20 MeV were used in this case.

For particle flux and energy deposition the following particle transport has been taken into account explicitly: p, n, d, t, α, ^{3}He, γ, μ, ν and π. We note separately that a total energy conservation has been checked carefully for all geometries. We model cylindrical homogeneous targets. The target radius is variable from 0.5 to 2.0 cm, and length from 10 to 50 cm. The proton source has Gaussian XY distribution (FWHM = 1.0 cm) and is directed parallel to Z axis (see Figure 1 for details). Energy of protons was always taken to be 1 GeV.

[1] A color print is recommended.

The target density was 19.3, 13.6 and 3.0 g/cm^3 for ^{nat}W, ^{nat}Hg and UC_x correspondingly (2.5 g/cm^3 of ^{238}U and 0.5 g/cm^3 of ^{12}C in UC_x).

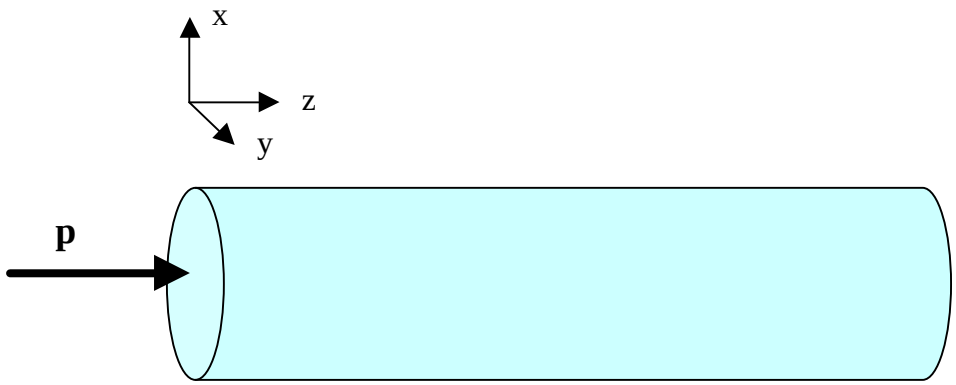

Fig. 1. *Configuration of target and proton source as modeled with MCNPX.*

Results (energy deposition)

Total energy deposition in (kW) at 1MW beam power is given in Table 1a-b as a function of different target configurations (materials and dimensions). In addition, the linear energy deposition was calculated for each cm of target length taking into account interaction of all transported particles excluding only neutrino. As the results do not significantly depend on the total length of the target, in the Figure 2 only energy deposition in the longest simulated target of each kind are given.

Table 1a. *Total energy deposition power (kW) in the cylindrical target from the 1MW beam.*

	p beam, (1 GeV) W target r=19.3 g/cm^3			**p beam, (1 GeV) Hg target r=13.6 g/cm^3**			**p beam, (1 GeV) UC_x target r=3.0 g/cm^3**		
l, cm	r=0.5cm	r=1cm	r=2cm	r=0.5cm	r=1cm	r=2cm	r=0.5cm	r=1cm	r=2cm
10	101	252	330	76	185	238	26	56	69
20	112	307	443	90	248	356	41	98	128
30	112	313	466	91	260	395	47	125	176
40	112	313	467	91	262	404	49	139	211
50	112	313	467	91	262	406	49	145	232
	UC_x target p beam, (0.5 GeV)			**UC_x target p beam, (2 GeV)**			**UC_x target ^{3}He beam, (2 GeV)**		
l, cm	r=0.5cm	r=1cm	r=2cm	r=0.5cm	r=1cm	r=2cm	r=0.5cm	r=1cm	r=2cm
10	55	120	141	16	36	46	43	91	106
20	77	201	262	27	66	88	71	164	199
30	82	236	349	34	88	123	82	213	277
40	83	248	396	37	102	150	86	239	338
50	83	252	418	39	111	172	88	252	378

Table 1b. *Total energy deposition power (kW) in the cylindrical low density target from the 1MW and 1 GeV proton beam.*

	CaO target r=0.35 g/cm^3			**Nb target r=2.5 g/cm^3**			**Ta target r=0.5 g/cm^3**		
l, cm	r=1cm	r=2cm	r=4cm	r=1cm	r=2cm	r=4cm	r=1cm	r=2cm	r=4cm
10	7	8	8	42	50	56	6	7	8
20	14	15	16	76	95	109	13	14	15
30	20	23	24	101	132	154	19	21	23
40	26	30	32	116	162	192	24	28	30
50	32	36	39	124	183	223	29	35	37
	ThC_4 target r=2.9 g/cm^3			**ThO_2 target r=1.71 g/cm^3**			**ThS_2 target r=1.28 g/cm^3**		
l, cm	r=1cm	r=2cm	r=4cm	r=1cm	r=2cm	r=4cm	r=1cm	r=2cm	r=4cm
10	45	55	62	24	29	32	19	22	24
20	80	103	120	46	56	63	36	43	47
30	103	142	169	62	81	92	50	62	69
40	114	170	209	73	102	118	60	79	90
50	120	188	241	80	118	141	67	94	108
	ZrC_4 target r=1.5 g/cm^3			**ZrO_2 target r=0.54 g/cm^3**					
l, cm	r=1cm	r=2cm	r=4cm	r=1cm	r=2cm	r=4cm			
10	28	32	36	9	10	11			
20	51	62	70	18	20	22			
30	70	88	101	26	30	32			
40	85	110	128	33	39	42			
50	95	128	152	40	47	52			

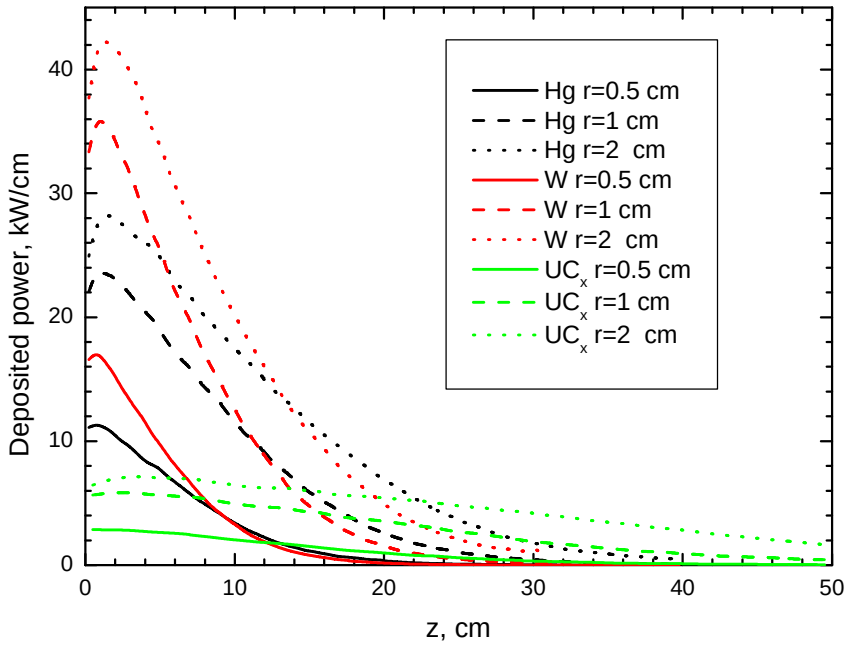

Figure 2. *Linear energy deposition (kW/cm) for different target configurations. Beam power is 1MW (1 GeV protons) in all cases. Also see Appendix.*

As seen from Figure 2 the maximum beam power deposition occurs at the first 1-3 cm from the target front surface and can exceed 40 kW/cm. One can observe maximum heating for W target, for Hg it is approximately 40% lower. Note that the difference in material density is of the same order of magnitude. Further from the Brag peak (for W at ~31cm and for Hg at ~45 cm) the calculated heat deposition becomes negligible and the total power dissipated in the target does not increase for longer targets (see Table 1 for details). For the UC_x mixture the heating power is more equally distributed along the entire target, and the maximum heating is only 7.1 kW/cm. In addition, 1 GeV protons are not fully stopped even for the longest target considered in this case (~50 cm).

It must be noted that due to the finite target diameter a significant fraction of beam protons and secondary particles are scattered off the target area. So for the thinnest target (r = 0.5 cm) almost all heating occurs in the first 20 cm for W target (corresponding length for Hg is 30 cm, and for UC_x – 40 cm).

For the spatial power deposition a cylindrical mesh tally (z step 0.5, r step 0.1 cm) was used integrating the total energy deposit over 360° azimuth angle. A contribution due to the primary proton beam was also separately evaluated as presented below.

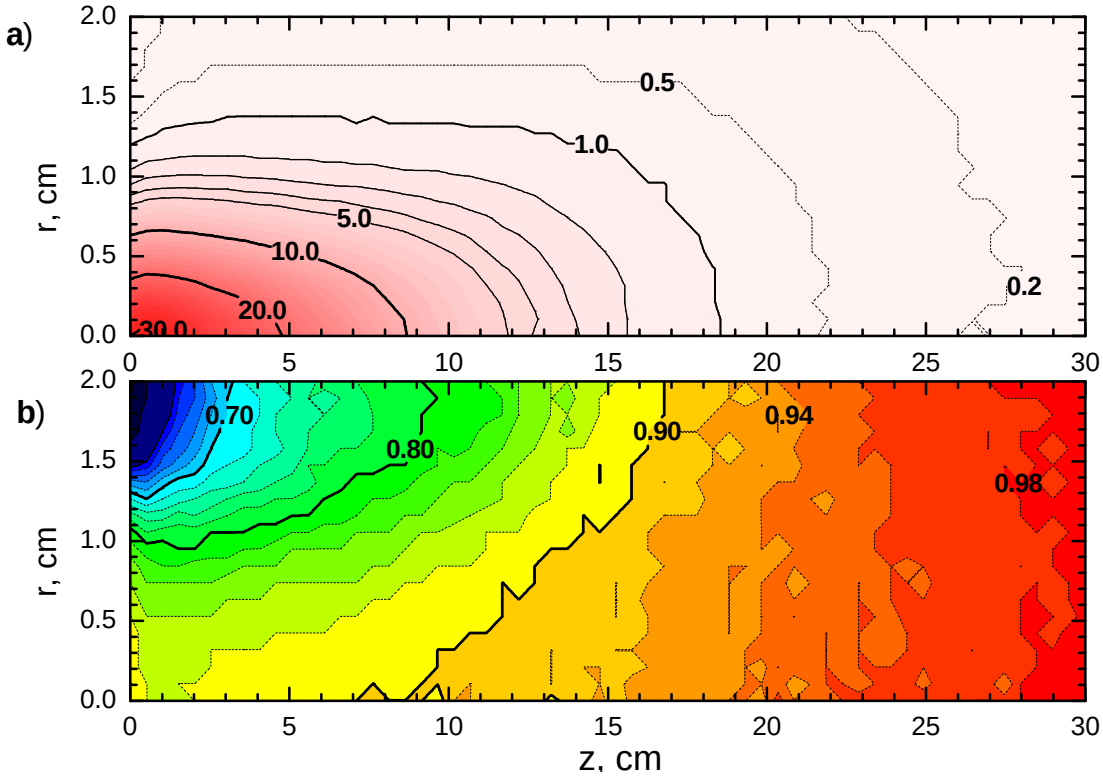

Figure 3. *Energy deposition in the W target (r=2 cm, l=30 cm):* ***a)*** *total heating power density in kW/cm^3,* ***b)*** *partial heating power induced by protons only.*

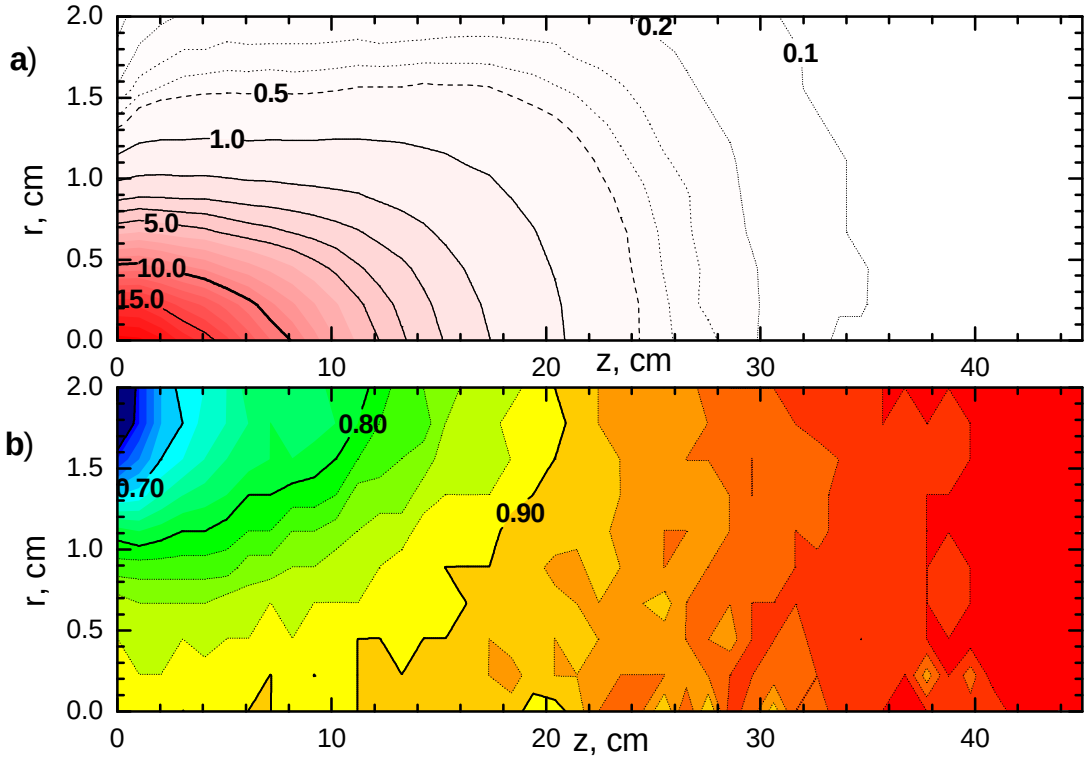

Figure 4. *Energy deposition in the Hg target (r=2 cm, l=50 cm):* ***a)*** *total heating power density in kW/cm*^{3}*,* ***b)*** *partial heating power induced by protons only.*

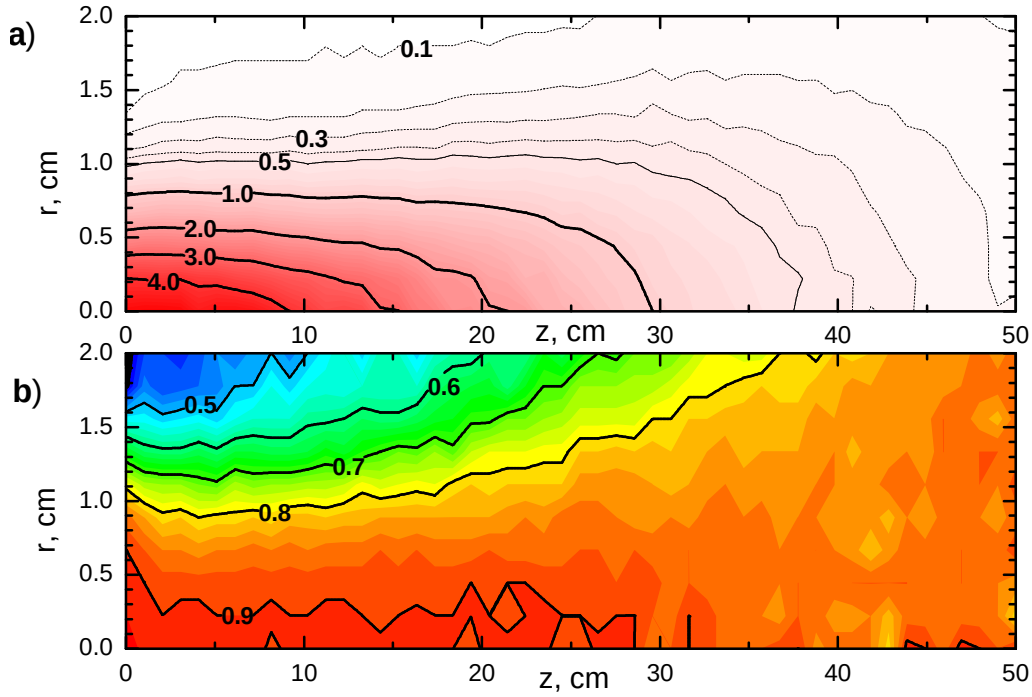

Figure 5. *Energy deposition in the UC_x target (r=2 cm, l=50 cm):* ***a)*** *total heating power density in kW/cm*^{3}*,* ***b)*** *partial heating power induced by protons only.*

To characterize a maximal local heating of the target in Fig. 6 we present the highest power density predicted along the beam axis. As it is seen from this representation, a very strong z-dependence is observed. Contrary, a maximal local power density is nearly independent of the target diameter as shown in Table 2.

Table 2. *Maximal local power density in the target. Beam power is 1MW with 1 GeV protons.*

	Hg	**W**	**UC_x**
r, cm	Power for unit volume, kW/cm^3		
0.5	19.3	29.3	4.8
1	19.9	30.6	4.9
2	20.1	30.7	4.9
	Power for unit mass kW/g		
0.5	1.42	1.52	1.59
1	1.47	1.59	1.65
2	1.48	1.59	1.62

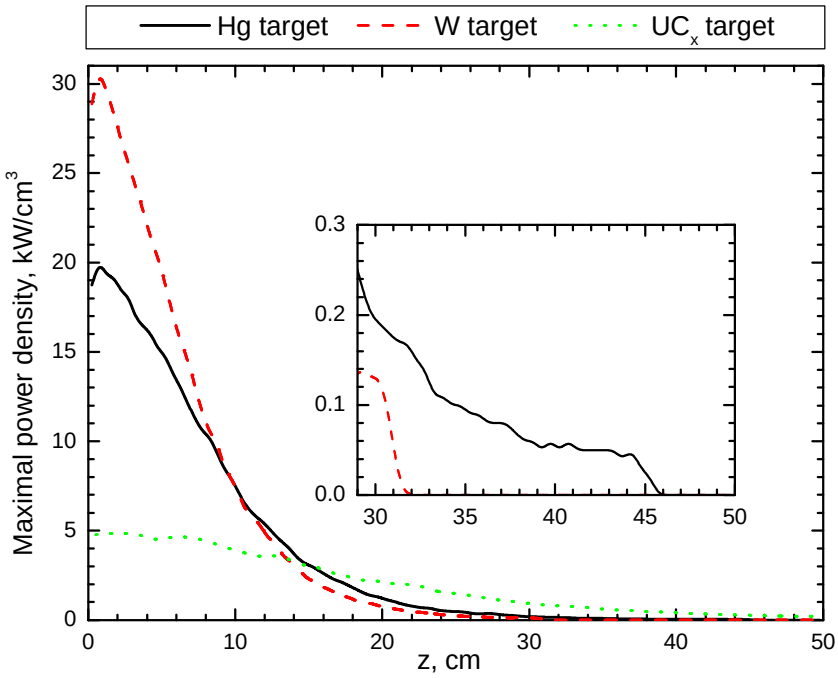

Figure 6. *Maximal local power density (kW/cm^3) in the target. Beam power is 1 MW with 1 GeV protons.*

Results (outgoing particles)

Neutron energy spectra (see below) have the maximum at ~3 MeV for the 0.5 cm radius targets in all materials. As long as the target diameter increases, this maximum shifts to lower values with an exception of UC_x due to its low density. In the case of targets with r = 2 cm the neutron flux reaches the maximum at ~1.5 MeV (W), ~2 MeV (Hg), ~3 MeV (UC_x) as shown in Figure 7. The 10 cm length W target emits already ~72% of all possible neutrons compared with longer targets of the same material. In other words, neutron production is nearly saturated in this case.

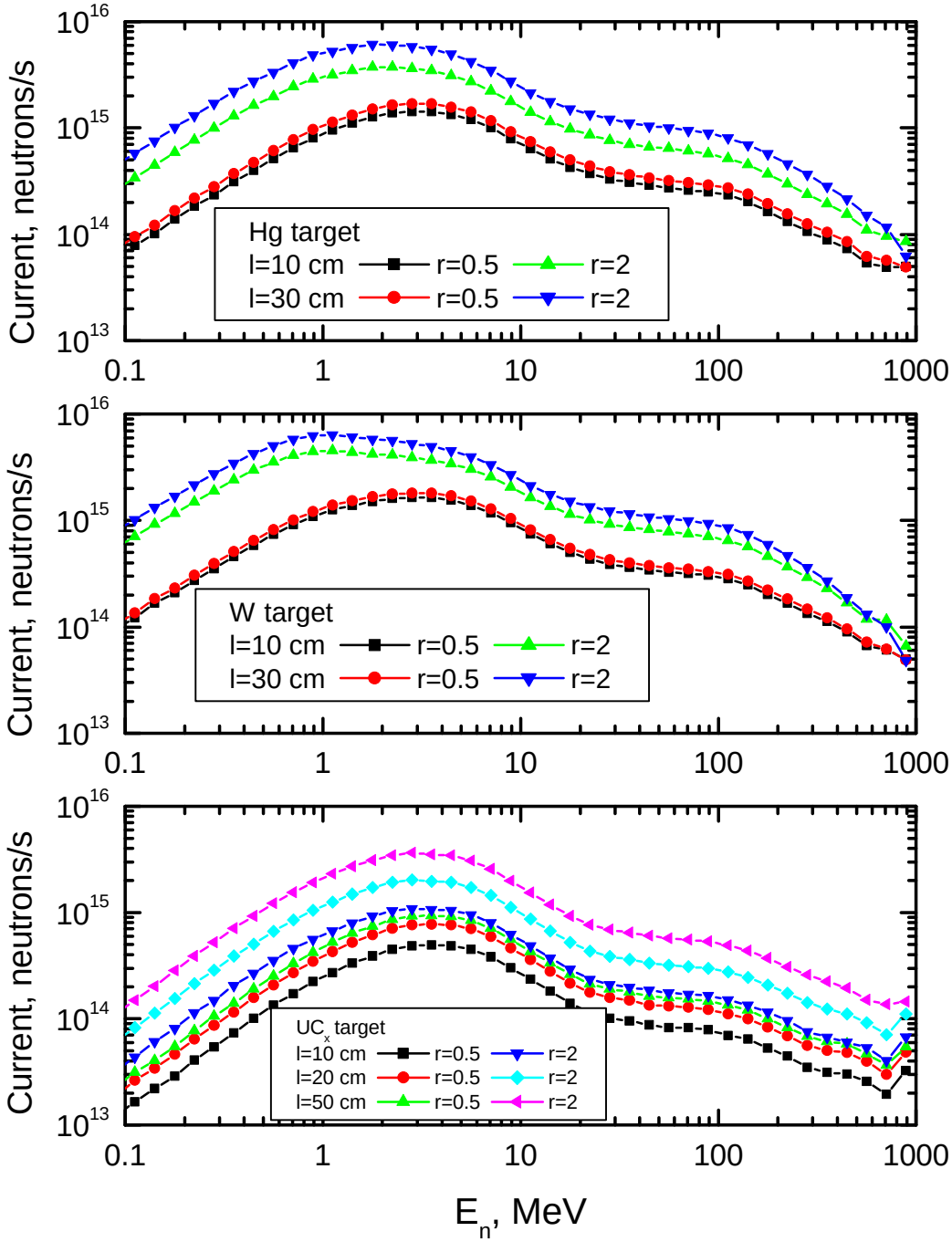

Figure 7. *Outgoing neutron energy spectra for different target configurations (see the legend).*

Photon energy distributions (see below) are peaked at ~1 MeV for all materials and all geometries. In addition, another (much lower in absolute value) peaking is observed at photon energies around 150 MeV, and its intensity decreases with target diameter (except UC_x due to its low density). These high energy photons originate from the pion decay process.

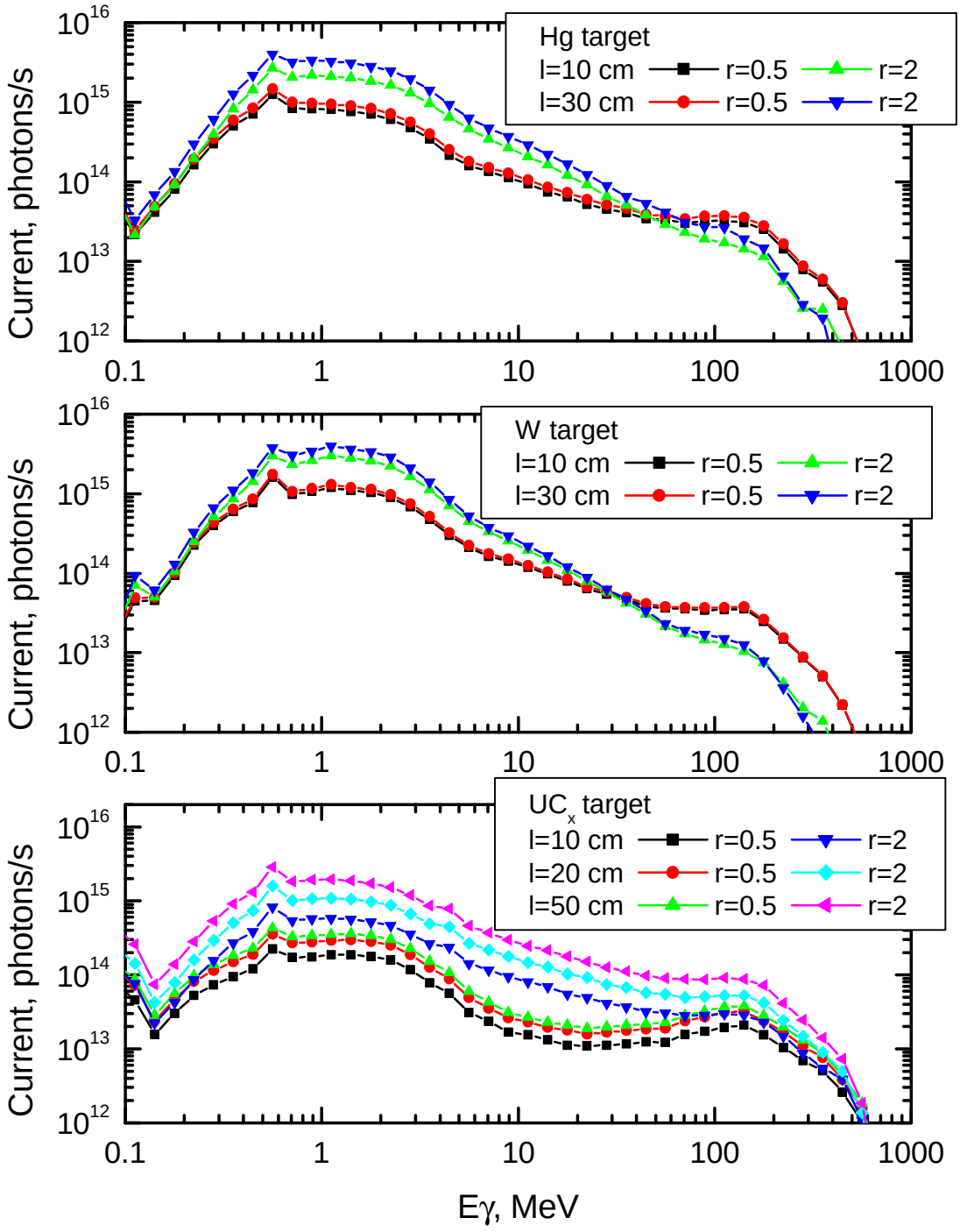

Figure 8. *Outgoing photon energy spectra for different target configurations (see the legend).*

Proton energy spectra (see below) are peaked close to the incident energy of 1 GeV. These are mainly primary source protons deviated from the target after a certain number of interactions. This peak shifts quickly to the lower energies for bigger target dimensions (both for a longer length and bigger diameter in particular).

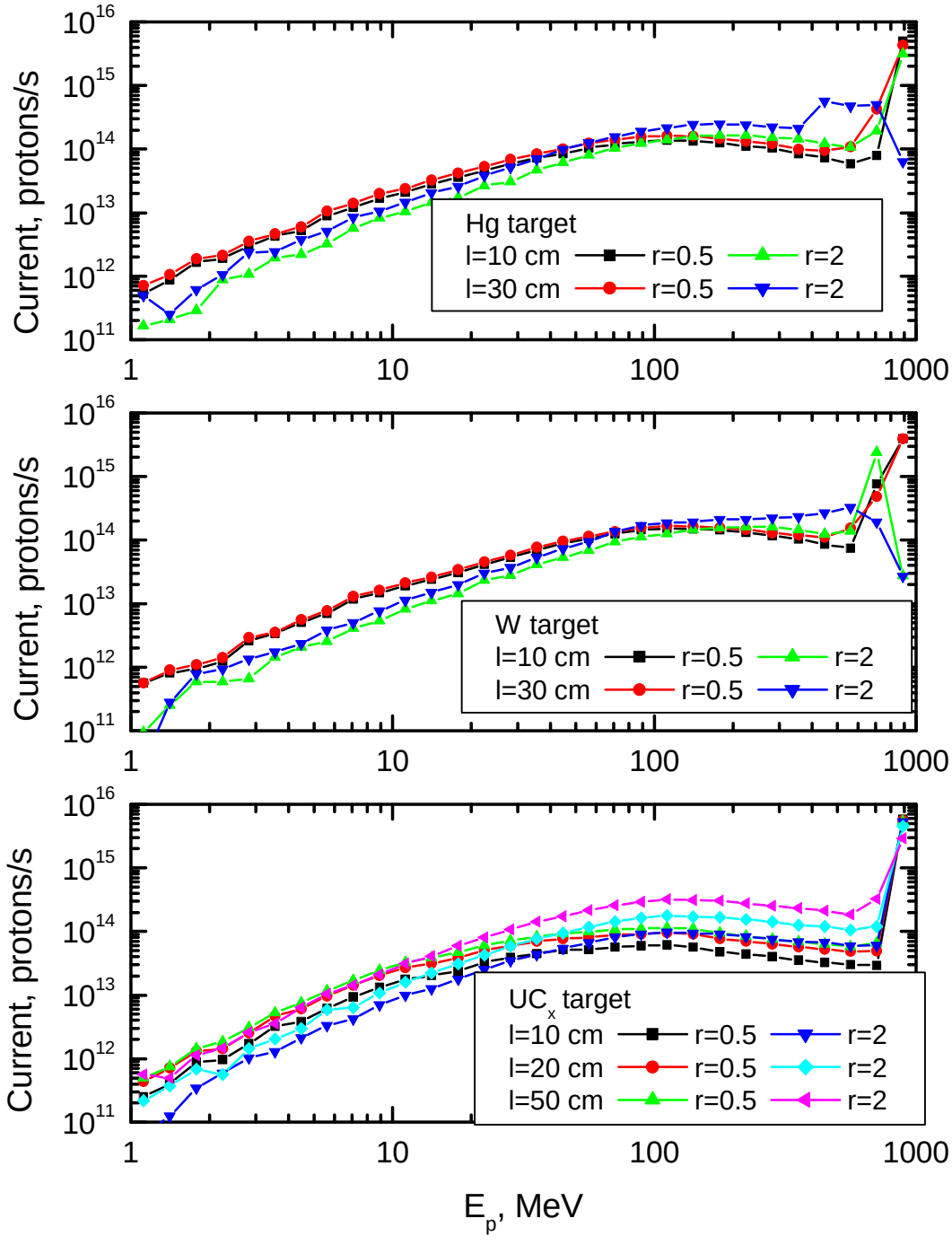

Figure 9. *Outgoing proton energy spectra for different target configurations (see the legend).*

Angular distributions of emitted particles were calculated on the 100 cm radius sphere, centered on the front side of each target independently on its dimensions. This sphere was divided into angular intervals in terms of solid angles in order to track the emitted particles. A direction of the proton beam (z-axis) was taken as a reference. For example, angles below 90^o correspond to the forward emission. As the target and beam configuration were axially symmetric, in all cases azimuth averaged distributions were calculated.

Figures 10 and 11 present angular distributions of neutrons emitted from different targets. In addition, the neutrons are grouped by certain energy intervals. It should be noted that most of the neutrons are nearly isotropic and fall into the energy range between 1 and 10 MeV (emitted through the evaporation process). Higher anisotropy is observed only for high energy (> 100 MeV) neutrons being strongly forward peaked. In general, angular distributions are very much target-geometry dependent in the case of low energy neutrons (due to the attenuation/deviation of neutrons interacting along the target), while for higher energy neutrons the angular distributions reflect more the neutron production process itself.

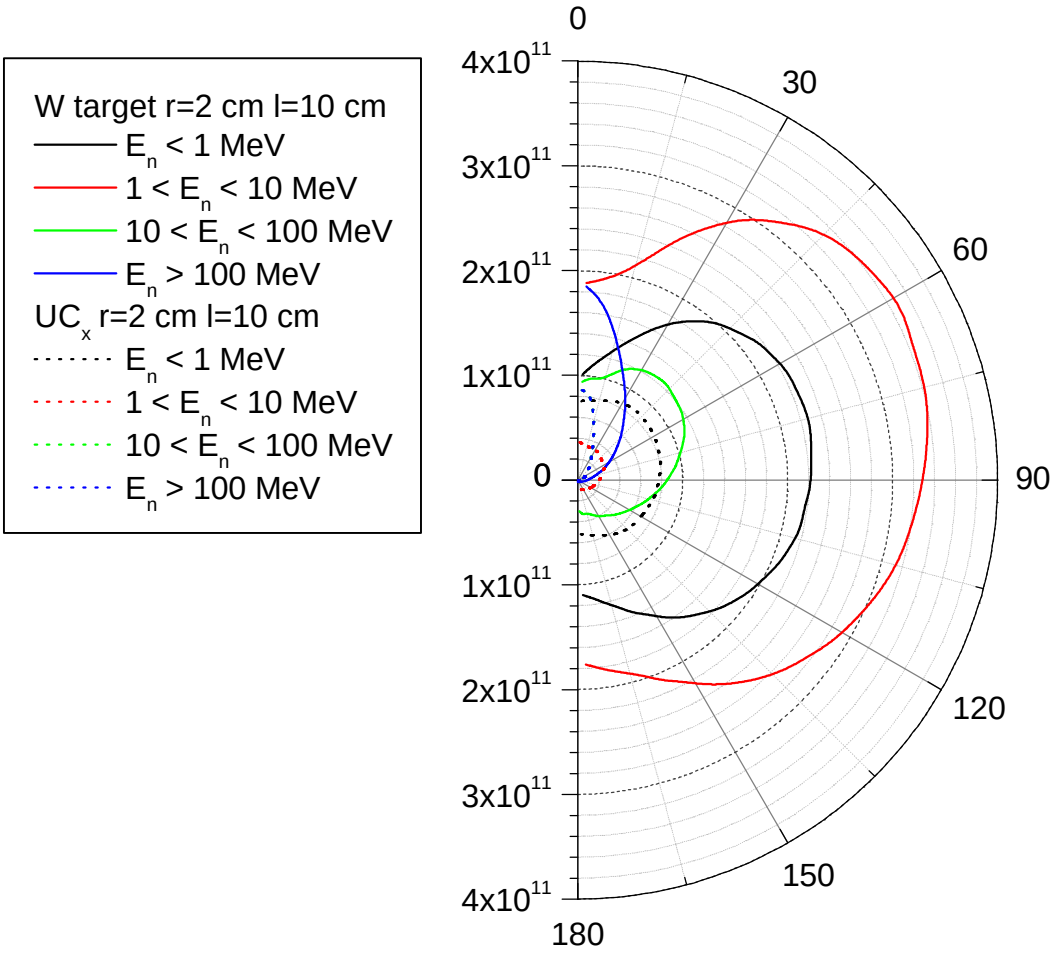

Figure 10. *Angular distribution of neutron flux (in n/(cm^2·s)) on the sphere with r=100 cm and centered on the front side of the target (short targets).*

For much longer and dense targets (compare below W and UC_x) neutron attenuation/deviation is seen for all energies, i.e. the neutron flux is minimal at forward angles (see solid lines). In the case of the UC_x target, high energy neutrons still preserve their initial forward direction.

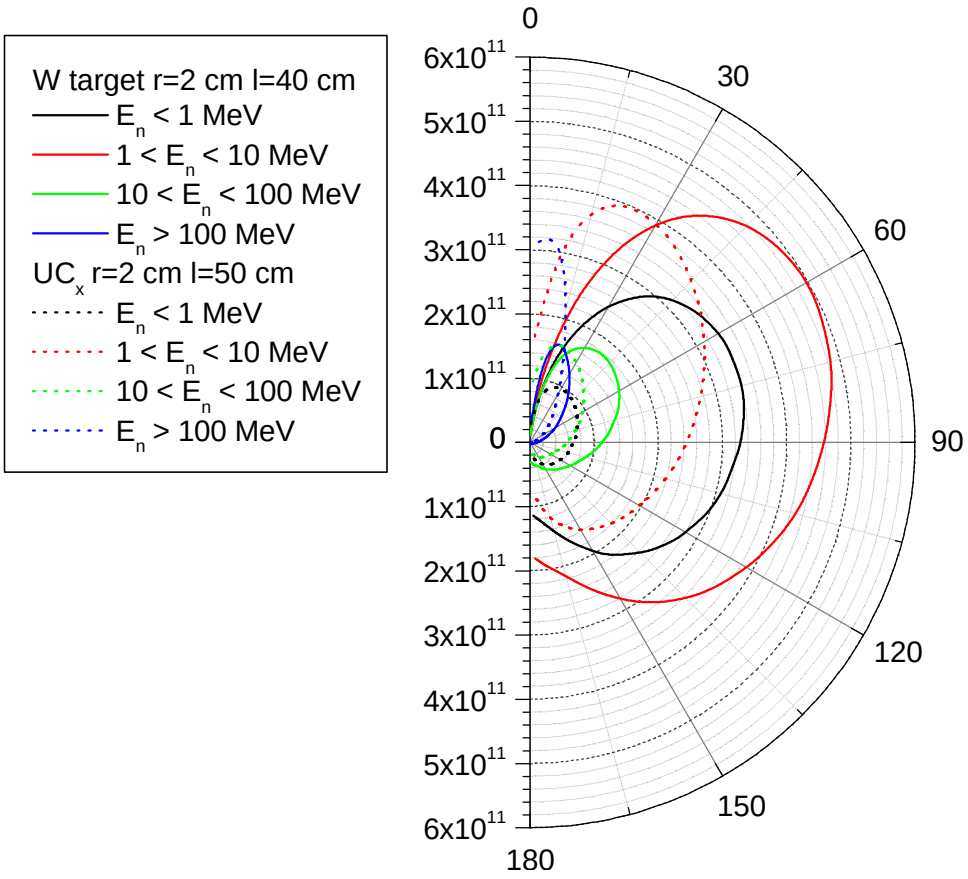

Figure 11. *Angular distribution of neutron flux (in n/(cm^2·s)) on the sphere with r=100 cm and centered on the front side of the target (long targets).*

An interesting feature is observed in the case of the angular dependence of emitted prompt photons[2] as presented below. As a matter of fact, there are no (little) photons at the very forward (backward) angles in the case of long/dense targets. Simply these photons, although produced all over the target, are strongly attenuated by the target material itself. This attenuation increases with target dimensions and density (compare, for example, photons emitted from W and UC_x).

[2] We note separately at this point that we neglected at the moment delayed photons, i.e. gammas originating from the radioactive decay of reaction products.

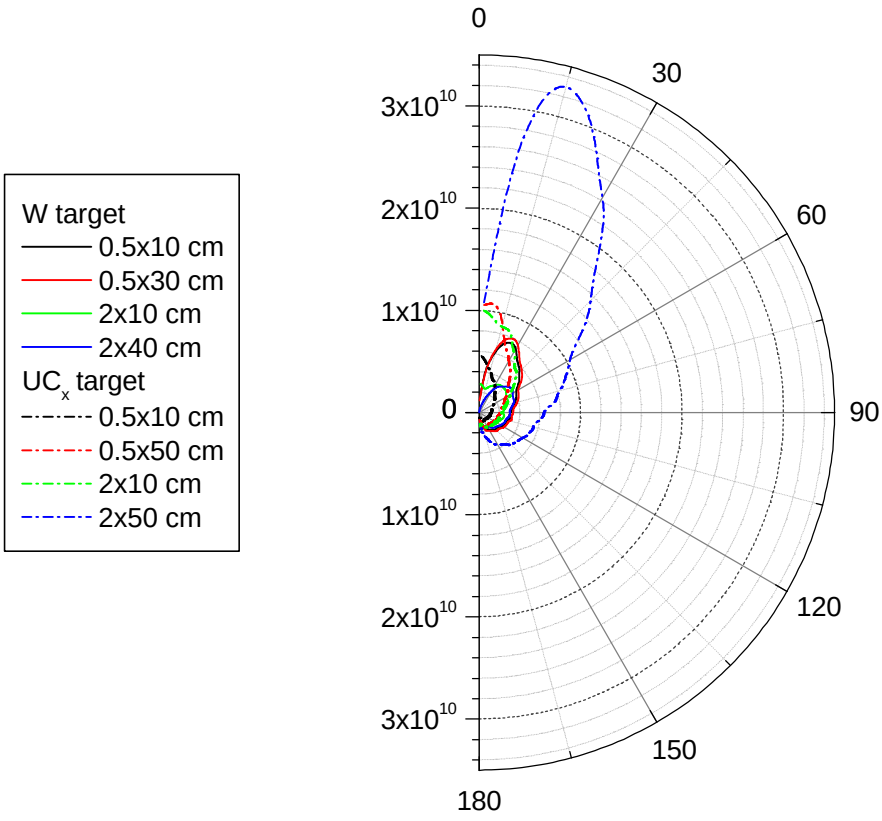

Figure 12. *Angular distribution of high energy E>20 MeV photons (in g/(cm^2·s)) on the sphere with r=100 cm and centered on the front side of the target.*

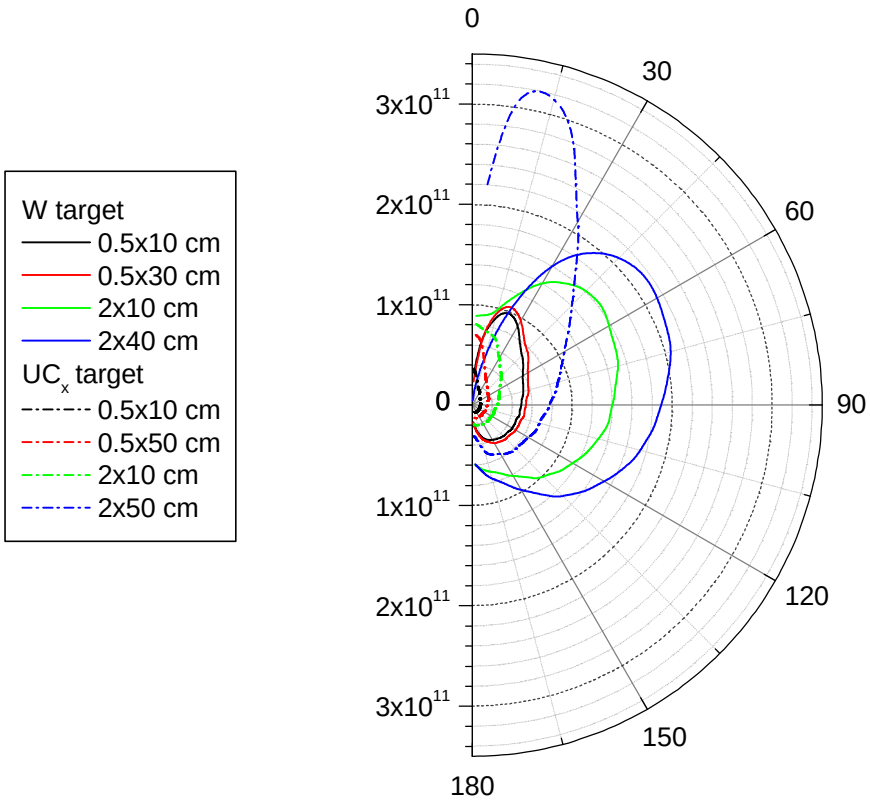

Figure 13. *Angular distribution of low energy E<20 MeV photons (in g/(cm^2·s)) on the sphere with r=100 cm and centered on the front side of the target.*

Finally, Figure 14 presents outgoing proton angular distributions. The most energetic protons, being primary beam protons, are strongly forward peaked. A sharp decrease in their flux is observed only for the targets extending further Brag's peak (see the blue solid line, for example).

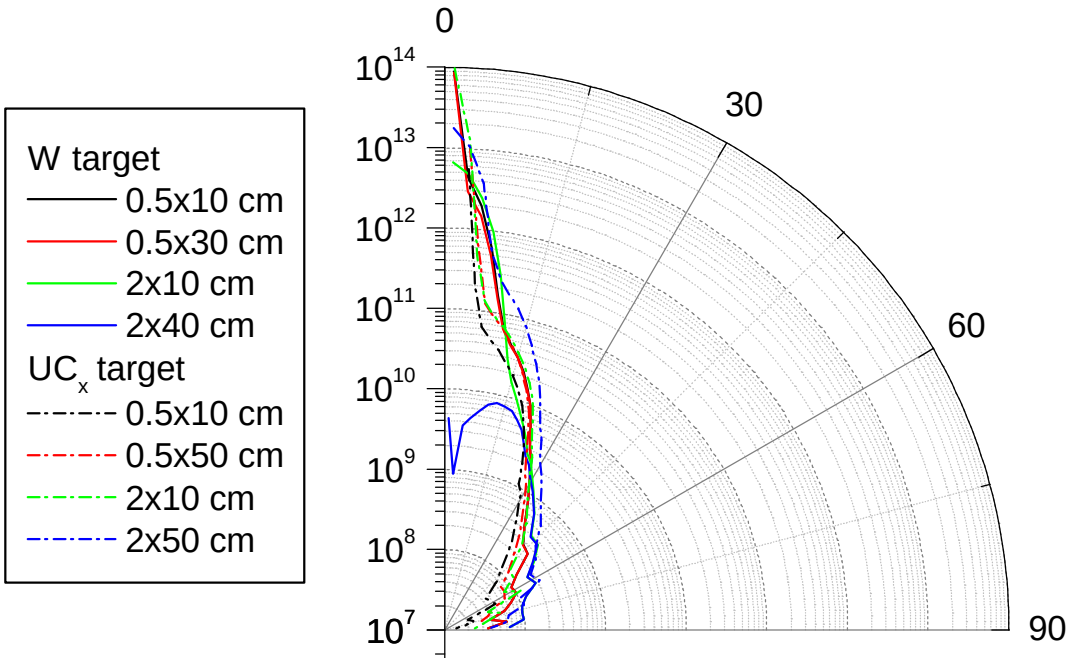

Figure 14. *Angular distribution of high energy (E>750 MeV) protons (in p/(cm^2·s)) on the sphere with r=100 cm and centered on the front side of the target. Note the logarithmic scale.*

Conclusions

The calculations of 1 GeV protons interacting with natural tungsten, mercury and UC_x as target materials have been performed. Our main observable was **A)** the total energy deposition including its spatial distributions all over the target, and **B)** the outgoing particle (p, n, ?) energy and angular dependence. The following conclusions are drawn:

A) Energy deposition

1. The part of beam power deposited in the Hg target is 13% for 0.5 cm radius target, 36% for r = 1 cm, and 55 % for r = 2 cm. In the case of W (and UC_x) the corresponding numbers are: 15% (and 6%) for r= 0.5 cm, 42% (and 16%) for r = 1 cm, 63 % (and 25%). In all cases approximately 90% of power is deposited by primary protons. Other non negligible contributors are photons and neutrons.
2. In the W target primary 1 GeV proton beam reaches ~31 cm, in the Hg target ~45 cm. In the low density UC_x target primary beam is not stopped even within 80 cm.
3. Maximal local power deposition in Hg is 20 kW/cm^3, in W -- 31 kW/cm3, and in UC_x -- 5 kW/cm^3. A corresponding maximal power for the unit mass is 1.5 kW/g for Hg and 1.6 kW/g for W and UC_x.

B) Outgoing particles

1. Outgoing neutron flux has the maximum at ~3 MeV for the 0.5 cm radius targets. In the case of r = 2 cm targets neutron flux reaches its maximum at ~1.5 MeV (W), ~2 MeV (Hg), and ~3 MeV (UC_x) correspondingly. Photons flux is maximal at ~ 1 MeV for all

targets. Protons are mainly emitted close to the incident energies being the primary beam particles.

2. Angular distributions of the outgoing neutrons are rather isotropic (except for the high energies) and much less target-size dependent than these of photons or protons. High energy protons are emitted mainly at the very forward angles, while photon emission at the beam direction is the lowest.

Acknowledgements

One of the authors, namely A.P., thanks the EURISOL project (EU contract No 50R349) for a financial support.

References

[1] European Isotope Separation On-Line Radioactive Nuclear Beam Facility (EURISOL); for more info see http://www.ganil.fr/eurisol/ (September 2002).
[2] D. Ridikas, W. Mittig, N. Alamanos , «RNB production with a powerful proton accelerator » , report DAPNIA-SPHN-2000-59, CEA Saclay (2000) ; available at http://www.ganil.fr/eurisol/CEA_RNB_production_paper.pdf (September 2002).
[3] L.S. Waters, "MCNPX^{TM} USER's MANUAL", Los Alamos National Laboratory, *preprint TPO-E83-G-UG-X-00001*, (November 1999), also see http://mcnpx.lanl.gov/.

Appendix

Table A1. *Total energy deposition power (kW/cm) for different target configurations. Proton beam energy is 1GeV and power 1MW.*

	W target r=19.3 g/cm^3			**Hg target r=13.6 g/cm^3**			**UC$_x$ target r=3.0 g/cm^3**		
z, cm	r=0.5cm	r=1cm	r=2cm	r=0.5cm	r=1cm	r=2cm	r=0.5cm	r=1cm	r=2cm
1	16.89	34.67	39.66	11.22	22.89	26.29	2.86	5.64	6.46
2	16.12	35.36	42.22	10.96	23.45	28.19	2.83	5.81	6.86
3	14.19	32.91	40.80	9.95	22.46	27.47	2.82	5.86	7.06
4	12.44	29.95	38.56	8.96	21.08	26.37	2.76	5.81	7.13
5	10.57	26.78	35.16	8.09	19.84	25.61	2.63	5.66	7.03
6	8.87	23.70	32.18	7.15	17.98	23.84	2.58	5.63	7.03
7	7.37	20.98	29.30	6.25	16.50	22.29	2.50	5.50	6.95
8	5.98	18.31	26.56	5.31	15.07	20.84	2.37	5.47	6.91
9	4.68	15.85	23.85	4.54	13.73	19.41	2.24	5.23	6.67
10	3.71	13.61	21.29	3.75	12.31	18.11	2.09	5.02	6.56
11	2.86	11.49	19.03	3.05	10.86	16.84	1.99	4.85	6.35
12	2.16	9.66	16.95	2.50	9.71	15.68	1.87	4.70	6.25
13	1.64	8.04	15.04	1.97	8.42	14.23	1.79	4.64	6.20
14	1.21	6.44	13.03	1.58	7.41	13.17	1.70	4.60	6.26
15	0.90	5.23	11.37	1.27	6.36	12.06	1.57	4.31	6.02
16	0.69	4.29	10.03	1.02	5.45	10.96	1.45	4.31	5.99
17	0.50	3.46	8.65	0.79	4.72	10.02	1.30	4.00	5.70
18	0.36	2.71	7.35	0.63	4.05	9.11	1.18	3.83	5.59
19	0.27	2.14	6.35	0.49	3.34	8.21	1.10	3.72	5.58
20	0.20	1.72	5.36	0.40	2.78	7.27	1.03	3.60	5.48

	W target r **=19.3 g/cm^3**			**Hg target** r **=13.6 g/cm^3**			**UC$_x$ target** r **=3.0 g/cm^3**		
21	0.15	1.34	4.49	0.30	2.36	6.54	0.92	3.45	5.36
22	0.11	1.05	3.78	0.23	1.93	5.75	0.82	3.28	5.24
23	0.09	0.84	3.18	0.18	1.62	5.06	0.74	3.14	5.17
24	0.06	0.68	2.64	0.13	1.33	4.43	0.72	2.99	5.00
25	0.04	0.53	2.22	0.10	1.16	3.93	0.61	2.73	4.83
26	0.03	0.42	1.87	0.09	0.92	3.37	0.55	2.60	4.68
27	0.02	0.36	1.59	0.07	0.79	2.96	0.49	2.50	4.63
28	0.01	0.29	1.39	0.05	0.62	2.53	0.42	2.32	4.48
29	0.01	0.24	1.22	0.04	0.53	2.19	0.40	2.14	4.36
30	0.01	0.22	1.17	0.03	0.43	1.89	0.34	1.97	4.29
31	0.01	0.19	1.00	0.02	0.36	1.67	0.31	1.82	4.08
32	0.00	0.01	0.06	0.01	0.31	1.43	0.28	1.72	3.94
33	0.00	0.00	0.02	0.01	0.25	1.21	0.26	1.61	3.84
34	0.00	0.00	0.01	0.01	0.20	1.07	0.24	1.52	3.64
35	0.00	0.00	0.01	0.01	0.17	0.95	0.20	1.39	3.51
36	0.00	0.00	0.00	0.01	0.13	0.81	0.17	1.29	3.40
37	0.00	0.00	0.01	0.00	0.11	0.72	0.17	1.19	3.29
38	0.00	0.00	0.01	0.00	0.10	0.62	0.14	1.08	3.10
39	0.00	0.00	0.01	0.00	0.08	0.54	0.14	1.07	2.99
40	0.00	0.00	0.00	0.00	0.06	0.47	0.13	0.95	2.86
41				0.00	0.05	0.42	0.11	0.90	2.77
42				0.00	0.05	0.39	0.09	0.78	2.54
43				0.00	0.04	0.36	0.07	0.71	2.46
44				0.00	0.04	0.36	0.08	0.68	2.32
45				0.00	0.04	0.33	0.07	0.64	2.25
46				0.00	0.01	0.06	0.06	0.60	2.08
47				0.00	0.00	0.00	0.05	0.54	2.00
48				0.00	0.00	0.00	0.04	0.48	1.89
49				0.00	0.00	0.00	0.04	0.42	1.75
50				0.00	0.00	0.00	0.03	0.42	1.64